

# The Silicon Vertex Detector of the Belle II Experiment

J. Wiechczynski,<sup>r,\*</sup> K. Adamczyk,<sup>r</sup> H. Aihara,<sup>p</sup> S. Bacher,<sup>r</sup> S. Bahinipati,<sup>e</sup>  
J. Baudot,<sup>d</sup> P. K. Behera,<sup>f</sup> S. Bettarini,<sup>j,k</sup> T. Bilka,<sup>b</sup> A. Bozek,<sup>r</sup> F. Buchsteiner,<sup>a</sup>  
G. Casarosa,<sup>j,k</sup> L. Corona,<sup>k</sup> S. B. Das,<sup>g</sup> G. Dujany,<sup>d</sup> C. Finck,<sup>d</sup> F. Forti,<sup>j,k</sup>  
M. Friedl,<sup>a</sup> A. Gabrielli,<sup>l,m</sup> B. Gobbo,<sup>m</sup> S. Halder,<sup>i</sup> K. Hara,<sup>q,n</sup> S. Hazra,<sup>i</sup>  
T. Higuchi,<sup>o</sup> C. Irmler,<sup>a</sup> A. Ishikawa,<sup>q,n</sup> Y. Jin,<sup>m</sup> M. Kaleta,<sup>r</sup> A. B. Kaliyar,<sup>a</sup>  
J. Kandra,<sup>b</sup> K. H. Kang,<sup>o</sup> P. Kodyš,<sup>b</sup> T. Kohriki,<sup>q</sup> R. Kumar,<sup>h</sup> K. Lalwani,<sup>g</sup>  
K. Lautenbach,<sup>c</sup> R. Leboucher,<sup>c</sup> J. Libby,<sup>f</sup> L. Martel,<sup>d</sup> L. Massaccesi,<sup>j,k</sup>  
G. B. Mohanty,<sup>i</sup> S. Mondal,<sup>j,k</sup> K. R. Nakamura,<sup>q,n</sup> Z. Natkaniec,<sup>r</sup> Y. Onuki,<sup>p</sup>  
F. Otani,<sup>o</sup> A. Paladino,<sup>A,j,k</sup> E. Paoloni,<sup>j,k</sup> K. K. Rao,<sup>i</sup> I. Ripp-Baudot,<sup>d</sup> G. Rizzo,<sup>j,k</sup>  
Y. Sato,<sup>q</sup> C. Schwanda,<sup>a</sup> J. Serrano,<sup>c</sup> T. Shimasaki,<sup>o</sup> J. Suzuki,<sup>q</sup> S. Tanaka,<sup>q,n</sup>  
F. Tenchini,<sup>j,k</sup> R. Thalmeier,<sup>a</sup> R. Tiwary,<sup>i</sup> T. Tsuboyama,<sup>q</sup> Y. Uematsu,<sup>p</sup> L. Vitale,<sup>l,m</sup>  
Z. Wang,<sup>p</sup> H. Yin,<sup>a</sup> L. Zani<sup>B,c</sup> and F. Zeng<sup>o</sup> (Belle-II SVD collaboration)

<sup>a</sup>Institute of High Energy Physics, Austrian Academy of Sciences, 1050 Vienna, Austria

<sup>b</sup>Faculty of Mathematics and Physics, Charles University, 121 16 Prague, Czech Republic

<sup>c</sup>Aix Marseille Université, CNRS/IN2P3, CPPM, 13288 Marseille, France, <sup>B</sup>presently at INFN Sezione di Roma Tre, I-00185 Roma, Italy

<sup>d</sup>IPHC, UMR 7178, Université de Strasbourg, CNRS, 67037 Strasbourg, France

<sup>e</sup>Indian Institute of Technology Bhubaneswar, Bhubaneswar 752050, India

<sup>f</sup>Indian Institute of Technology Madras, Chennai 600036, India

<sup>g</sup>Malaviya National Institute of Technology Jaipur, Jaipur 302017, India

<sup>h</sup>Punjab Agricultural University, Ludhiana 141004, India

<sup>i</sup>Tata Institute of Fundamental Research, Mumbai 400005, India

<sup>j</sup>Dipartimento di Fisica, Università di Pisa, I-56127 Pisa, Italy, <sup>A</sup>presently at INFN Sezione di Bologna, I-40127 Bologna, Italy

<sup>k</sup>INFN Sezione di Pisa, I-56127 Pisa, Italy

<sup>l</sup>Dipartimento di Fisica, Università di Trieste, I-34127 Trieste, Italy

<sup>m</sup>INFN Sezione di Trieste, I-34127 Trieste, Italy

<sup>n</sup>The Graduate University for Advanced Studies (SOKENDAI), Hayama 240-0193, Japan

<sup>o</sup>Kavli Institute for the Physics and Mathematics of the Universe, University of Tokyo, Kashiwa 277-8583, Japan

<sup>p</sup>Department of Physics, University of Tokyo, Tokyo 113-0033, Japan

<sup>q</sup>High Energy Accelerator Research Organization (KEK), Tsukuba 305-0801, Japan

<sup>r</sup>H. Niewodniczanski Institute of Nuclear Physics, Krakow 31-342, Poland

E-mail: [wiechczynski@belle2.ifj.edu.pl](mailto:wiechczynski@belle2.ifj.edu.pl)

\*Speaker

36 The Belle II experiment operating at the asymmetric-energy  $e^+e^-$  SuperKEKB collider, located in Tsukuba (Japan), has been collecting data since March 2019. Its excellent vertexing abilities are provided by the vertex detector, part of which is the silicon-strip vertex detector (SVD) that plays a crucial role in the charged-particle tracking close to the interaction point. The SVD has operated successfully and efficiently over the whole period of data taking so far. In this article, we briefly discuss its purpose, structure and basic description of the front-end electronics. The main quantities related to the SVD performance are presented. The foreseen increase in SuperKEKB luminosity will lead to higher background, so we describe its impact on the SVD performance. A quick overview of the radiation damage campaign is presented to show the predicted behaviour of the sensors subjected to high radiation, whose level is constantly monitored. We also discuss the ongoing software development to account for the high occupancy expected in the future. In particular, the utilization of the SVD hit time information is presented as a very important quantity to suppress off-time background hits and tracks. Finally, the work done during the first long shutdown of SuperKEKB is briefly described, during which a major upgrade of the pixel detector has been successfully done. Resumption of the beam operation is expected in early 2024.

Keywords: Silicon strip detector, Vertex detector, Tracking detector, Belle II

## 1. Introduction

The Belle II [1] experiment is dedicated to search for physics beyond the standard model at the intensity frontier. It operates at the SuperKEKB collider located at KEK, Tsukuba in Japan, providing asymmetric beams of 7 GeV electrons and 4 GeV positrons. In the accelerator's default operation regime, the center-of-mass energy is set to the  $\Upsilon(4S)$  resonance, hence it produces a huge sample of  $B$  mesons via the  $e^+e^- \rightarrow \Upsilon(4S) \rightarrow B\bar{B}$  process. So far, SuperKEKB achieved the highest instantaneous luminosity of  $4.7 \times 10^{34} \text{ cm}^{-2}\text{s}^{-1}$ , which is the current world record. The Belle II detector is a multipurpose spectrometer characterized by excellent vertexing capability and good hermeticity, which has accumulated  $424 \text{ fb}^{-1}$  to date, and its final goal is to collect a data sample of  $50 \text{ ab}^{-1}$ , that will be possible with a constant increase of the SuperKEKB instantaneous luminosity up to our final goal of  $6 \times 10^{35} \text{ cm}^{-2}\text{s}^{-1}$ .

Belle II is composed of various sub-detectors with the vertex detector (VXD) being the closest to the interaction point. It is divided into two further subsystems. The innermost part is the pixel detector (PXD), which is based on depleted field effect transistor pixel sensors. The PXD consists of two layers (numbered 1-2) and its main goal is the precise determination of the decay vertices. Outside the PXD is the silicon-strip vertex detector (SVD) [2] with four layers (numbered 3-6) that mostly extrapolates the measured tracks to the PXD, defining the so-called region of interest (ROI), which significantly reduces the amount of data recorded by the PXD. The SVD also performs standalone tracking for low-momentum charged particles and contributes to their identification by providing energy loss information.

## 2. SVD structure

Each SVD layer is composed of a number of double-sided silicon strip detectors (DSSDs) that are manufactured on an n-type bulk wafer with a thickness of about  $300 \mu\text{m}$  (Figure 1). One side of the sensor is covered by the p-type silicon strips placed in parallel to the beam axis that determine the  $r - \phi$  coordinates (distance from the  $z$ -axis and azimuthal angle, respectively), and the n-type strips are placed perpendicularly on the other side of the bulk, measuring the  $z$  coordinate (collinear to the electron beam). Figure 1 (left) shows a schematic picture of SVD layers and associated sensors with increasing numbering from the forward (FWD) to the backward (BWD) regions. Such structure is repeated along the azimuthal direction forming different ladders and the so-called windmill geometry of the SVD. The sensors differ depending on the layer and the region in which they are placed in the SVD. In the FWD part, for layers 4-6, they have a trapezoidal shape

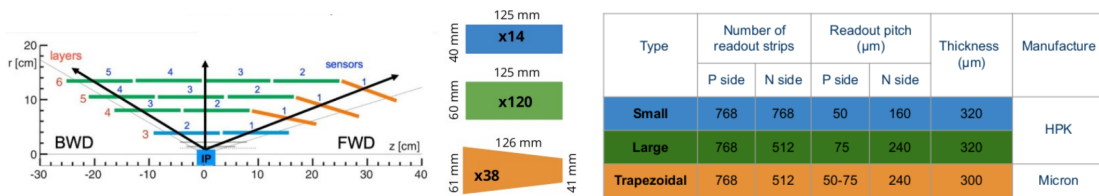


**Figure 1:** Schematic picture of SVD sensors forming different layers (left) and a table summarizing the parameters for each type of sensor (right).

68 and are slanted in the region that, due to the asymmetric beams, is characterised by the highest track  
69 multiplicity. In addition, in layer 3 the sensors are smaller and contain more n-type strips than that  
70 in layers 4-6. This also implies the readout pitch (distance between two readout strips) to be much  
71 smaller for p-side strips with respect to the n-side. To improve spatial resolution, a floating strip is  
72 placed between two readout strips on both p- and n-sides. The charge induced in the floating strip  
73 is shared by the neighboring strips, reducing the effective strip pitch to half of the readout pitch.  
74 The right table of Figure 1 summarises the sensor parameters. The SVD consists of 224 thousand  
75 readout strips and 172 sensors with an active area of 1.2 m<sup>2</sup>.

## 76 2.1 Front-end electronics

77 For the readout we use APV25 chips [3]. For the central part of SVD (except for layer 3), the  
78 chips are attached directly to the DSSD sensors via flex circuits bent over the DSSD edge (Origami  
79 concept). The edge sensors use hybrid boards located outside the active volume. The APV25 has  
80 128 channels per chip and amplifiers that provide a shaping time of 50 ns. Radiation hardness  
81 exceeds 100 Mrad and the power consumption is around 0.4 W/chip. The sampling frequency is 32  
82 MHz and after the trigger's arrival we can collect six consecutive signal samples in total with the  
83 multipeak mode. To account for higher luminosity in the future, we have introduced the so-called  
84 "3/6 mixed acquisition mode", which allows switching between three and six samples recorded on  
85 an event-by-event basis, based on the trigger type (and hence its time accuracy) for a particular  
86 event. This mode, already prepared and tested, significantly reduces the data size, which can be  
87 crucial in high background conditions.

## 88 3. SVD performance

89 Since the start of the operation we have observed very smooth performance of the SVD, with a  
90 very few masked strips (less than 1%). Moreover, the environment has been stable and the evolution  
91 of calibration constants is consistent with expectation. Also, the effects of radiation damage are  
92 well under control.

93 Several quantities related to the SVD performance - sensor efficiency, signal-to-noise ratio, and  
94 both spatial and time resolution - are constantly monitored. Regarding SVD sensor efficiency, the  
95 values for all sensors are typically over 99% and they are also very stable over the whole period of  
96 data taking. Clusters are formed from adjacent strips with significant signal and the charge collected  
97 in a given cluster strongly depends on the incident angle of the track. Over time, we observe very  
98 similar cluster charge in all the sensors once normalized to the track's length. For layer 4-5-6 on  
99 the n-type strips we observe 10-30% loss of the signal due to the large pitch combined with the  
100 presence of a floating strip. Another important quantity is the signal-to-noise ratio (SNR), which is  
101 satisfactory for all 172 sensors. The SNR MPV is ranging from 13 to 30, depending on the sensor  
102 position, due to the track incident angle with the sensor, and on the sensor side, with smaller SNR  
103 for the p-sides, due to larger noise for the longer strip length. A small decrease of cluster SNR value  
104 is observed in 2022 measurement, due to increased noise from radiation damage by approximately  
105 20%-30%. In Figure 2 the distributions of cluster charge (left) and SNR (right) are presented,  
106 where histograms representing the data collected in 2020 and 2022 are superimposed.

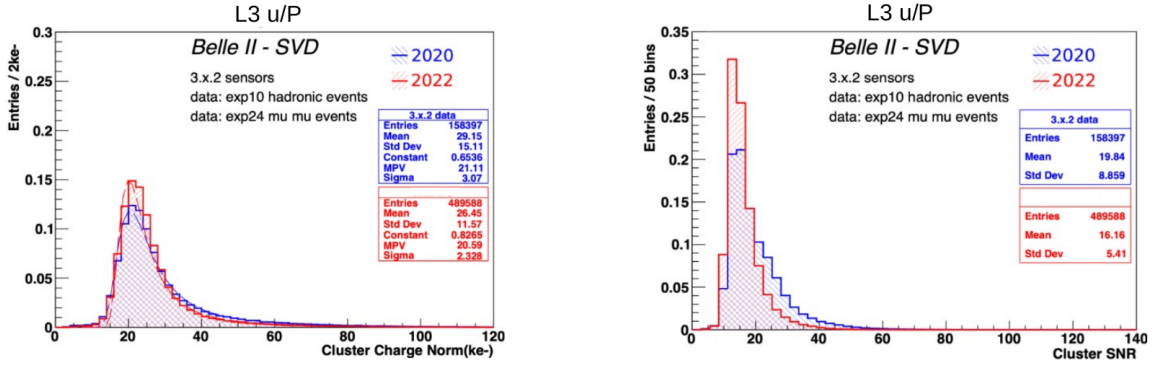


**Figure 2:** Distribution of cluster charge (left) and signal-to-noise ratio (right) for layer 3 (p-side). Comparison between data taken in 2020 (blue) and 2022 (red) is presented.

107 Both position and time resolution are very important metrics for excellent SVD performance.  
 108 The position resolution measurement is based on the residuals, i.e., the clusters' positions with  
 109 respect to the intercept of the unbiased tracks' extrapolation, and it is evaluated with a large sample  
 110 of  $e^+e^- \rightarrow \mu^+\mu^-$  decays. As shown in Figure 3, this quantity depends on the incident angle and  
 111 is very stable during the period of the Belle II operation. Cluster position is calculated as the  
 112 center of gravity [4] (i.e. weighted mean) of the various strip positions inside the cluster, using the  
 113 collected charge as the strip weight. The cluster position resolution then depends on cluster size  
 114 and on the strip signal-to-noise ratio. These quantities vary with track incident angle, which results  
 115 in the non-monotonic dependence of the resolution seen in Figure 3. For zero incident angle, with  
 116 perpendicular tracks more likely to produce a single strip cluster, one can only achieve a "digital  
 117 resolution", i.e., floating strip pitch/ $\sqrt{12}$ . The resolution improves with more than one strip in the  
 118 cluster because of the charge-weighted average analog information. It reaches a minimum for two  
 119 strip clusters, which corresponds to an incident angle where the projection of the track along the  
 120 direction perpendicular to the strips on the detector plane is two floating strip pitches (4 and 14  
 121 degrees for the layer 3 p- and n-sides pitches). For large incident angles, since the signal collected  
 122 in each strip decreases with the incident angle  $\theta$  (proportional to  $\text{pitch}/\sin(\theta)$ ), the consequent  
 123 reduction of the strip signal-to-noise ratio degrades the cluster position resolution. In general, the  
 124 resolution for the n-side (right plot) is about two times worse with respect to that for the u-side,  
 125 which is a result of the different pitch and strip signal-to-noise ratio on the two sides.

126 Hit time resolution is measured with respect to the event time of the collision provided by  
 127 central drift chamber (CDC) and exhibits a very good resolution of less than 3 ns for the clusters  
 128 associated to tracks. Using the average value of all the hits on a given track, the so-called "track-  
 129 time" can be computed, slightly improving the time resolution. Furthermore, the "event-time"  
 130 can be determined using all the clusters associated to selected tracks in an event. In such a way,  
 131 the "event time" can be computed by the SVD with a resolution of the order of 1 ns, while the  
 132 computation is around 2000 times faster than the one based on CDC. This feature will be especially  
 133 important in the higher luminosity environment, as it can significantly speed up the reconstruction  
 134 process at the high-level trigger.

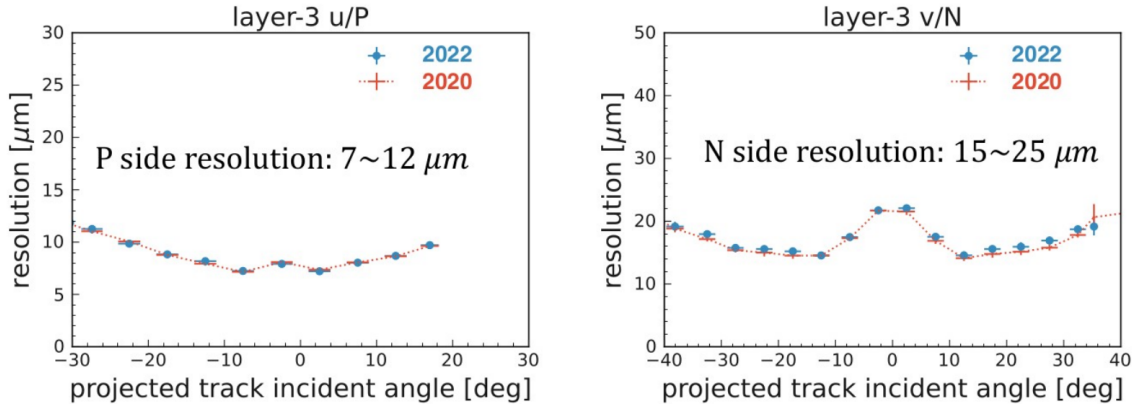


**Figure 3:** Distributions of position resolution for *p*-side (left) and *n*-side (right) as a function of the track incident angle. A comparison between data taken in 2020 (dots) and 2022 (dotted lines) is presented.

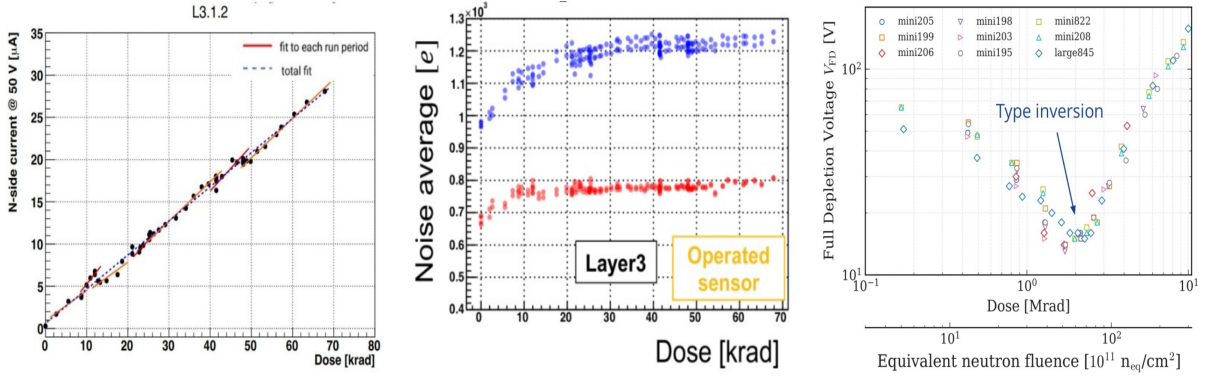


**Figure 4:** Left plot: Leakage current as a function of the accumulated dose; Center plot: the average noise level as a function of the accumulated dose for the *p*-side (blue dots) and *n*-side (red dots); Right plot: full depletion voltage as a function of the accumulated dose with the type inversion observed at 2 Mrad.

#### 135 4. Radiation effects

136 In the high-energy physics experiments, the effects from radiation damage coming from ma-  
 137 chine related background is a major factor that **degrades** the sensor performance with time. The  
 138 SVD accumulated dose is constantly measured using data from diamond sensors that are mounted  
 139 on the IP beam pipe, and the corresponding level of the equivalent neutron fluence is evaluated using  
 140 the ratio of equivalent neutron fluence to dose estimated from Monte Carlo simulation. Several  
 141 effects related to radiation damage must be taken into account. A linear increase of the leakage  
 142 current as a function of radiation damage is observed in the sensors, as expected from the bulk  
 143 damage described by the NIEL model [5], and shown in Figure 4 left. The sensor current is shown  
 144 as a function of the accumulated dose for one of the layer 3 sensors most exposed, that received  
 145 about 70 krad to date, corresponding to an equivalent neutron fluence of about  $1.6 \times 10^{11} \text{ n}_{\text{eq}}/\text{cm}^2$ .  
 146 So far, this increase has had a negligible contribution to the noise because of both the small leakage

147 current and the short APV25 shaping time. The rate of the leakage current increase measured  
148 is consistent with the experience from other experiments working with similar detectors and in  
149 comparable conditions [6]. However, we expect some significant impact on the strip noise due to  
150 the sensor leakage current, and hence a deterioration in SNR, for the dose of  $\sim 6$  Mrad, which is  
151 **considered** as SVD dose limit to preserve optimal performance. The strip noise for unirradiated  
152 modules is dominated by the interstrip capacitance. During the operation we have observed an  
153 increase in its value of about 20% (30%) for n-side (p-side), due to effects of surface radiation  
154 damage that increases the interstrip capacitance, but it is expected to saturate, as also visible in  
155 Figure 4 center.

156 Another relevant effect of the bulk radiation damage is the impact on depletion voltage.  
157 The expected future radiation levels at the nominal luminosity, of about 0.35 Mrad/year and  $8 \times$   
158  $10^{11}$   $n_{\text{eq}}/\text{cm}^2/\text{year}$ , are affected by large uncertainty due to the machine evolution as well as a  
159 possible redesign of the interaction region. To better explore the possible effects of bulk damage in  
160 the SVD sensors after bulk type inversion, an irradiation campaign was conducted in July 2022 at  
161 ELPH, Tohoku University. Several SVD sensors have been exposed to a 90 MeV electrons beam,  
162 up to 10 Mrad, corresponding to an equivalent neutron fluence of  $3 \times 10^{13}$   $n_{\text{eq}}/\text{cm}^2$ . The decrease  
163 of the depletion voltage has been observed up to the point of bulk type inversion, which occurred at  
164 2 Mrad ( $\sim 6 \times 10^{12}$   $n_{\text{eq}}/\text{cm}^2$ ), after which the depletion voltage started to increase again (Figure 4  
165 right). Detailed measurements, whose results will be shortly published, confirmed that the sensors  
166 will still work fine after the type inversion, which meets our expectation for these types of silicon  
167 detectors. Since the beginning of the detector operation, we have not observed any change in the  
168 depletion voltage in the sensors installed in the SVD, as expected due to the small accumulated  
169 equivalent neutron fluence so far, below  $2 \times 10^{11}$   $n_{\text{eq}}/\text{cm}^2$ . Considering all these results, the dose  
170 limit of 6 Mrad and the extrapolation of the background levels quoted above, the SVD has a wide  
171 safety margin for the accumulated radiation damage even after 10 years of the operation at the target  
172 luminosity.

## 173 5. High background scenario and related software/hardware developments

174 With the increase of the luminosity and the expected larger machine related background, the  
175 SVD occupancy will also increase and a deterioration of the tracking performance is expected above  
176 certain levels. So far, the average hit occupancy is 0.5% for layer 3, which does not degrade the  
177 performance. Nonetheless, the background extrapolation for different future scenarios has been  
178 performed with detailed simulations of the various contributions (beam-gas, Toushek, etc.) and  
179 applying appropriate data-simulation scale factors [7]. These studies predict that for the nominal  
180 luminosity we can reach an occupancy in layer 3 very close to the limit of 4.7%, above which the  
181 tracking performance deteriorates. These predictions have large uncertainties coming from poorly  
182 known machine evolution in the future, with a possible redesign of the interaction region. In the  
183 most conservative scenario, the layer-3 occupancy can increase up to  $\sim 8.7\%$ , which is far beyond  
184 the modest tracking performance. Such a scenario motivates us to develop the SVD reconstruction  
185 software, as well as to seriously consider the VXD upgrade [8], since the safety factor might be too  
186 small to ensure good quality data. The technology assessment related to this hardware upgrade is  
187 currently ongoing.

188 An important effort related to the software development is the utilization of the hit time  
189 information from the SVD. The real signal hits come from well-triggered collisions, but the SVD  
190 acquisition window ( $\sim 100$  ns) is much wider with respect to the SuperKEKB bunch spacing (6 ns).  
191 Therefore, we need to cope with many off-time hits related to the beam-induced background or  
192 background from the other bunches. The current selection is based on two requirements: a) time  
193 difference between p- and n-side cluster,  $|t_p - t_n| < 20$  ns, and b) the absolute value of the cluster  
194 time,  $|t_{p,n}| < 50$  ns. These criteria reject the majority of the background hits retaining above 99% of  
195 the signal, and based on them the SVD occupancy limit for layer 3 can be set at 4.7%. Recently, a  
196 more effective background suppression method has been developed in the form of so-called “SVD  
197 grouping”. It is based on an event-by-event classification of the clusters by their time, so the  
198 clusters belonging to tracks from the same collisions are collected in the same group. Clusters  
199 from the different collisions or beam background will be placed in the other groups; finally, only  
200 the clusters belonging to the priority group will be used for the tracking. This feature reduces the  
201 fake rate (fraction of the fake tracks) by 16% for the high-background scenario. An additional fake  
202 rate reduction can be achieved by applying the selection on the track-time to reject off-time tracks.  
203 Finally, these improvements allow an increase of the SVD occupancy limit for layer 3 from 4.7% to  
204 around 6%.

## 205 6. Activities during the Long Shutdown 1

206 Long shutdown 1 (LS1) started in May 2022 and one of the goals was to upgrade the VXD with a  
207 new PXD. During the first data taking period, the second layer of PXD was only partially equipped,  
208 and 5/6 of the azimuthal angle remained uncovered. The new PXD provides the full coverage,  
209 which is beneficial for more precise vertexing. Hardware activities for the VXD uninstallation and  
210 reinstallation were intense: after the VXD extraction from Belle II, the SVD was detached from  
211 the old PXD (May 16-17, 2023), then the new PXD was attached to the SVD (June 20-21, 2023)  
212 and finally the complete VXD was installed in the Belle II detector. The whole delicate procedure  
213 had neither major problems nor caused any damage. In the period of September 12 - October 1,  
214 2023, the VXD commissioning was performed to confirm the PXD and SVD performance, and  
215 also to check the impact from the increased PXD power consumption and possible increase in  
216 the temperature on the sensor leakage current. From September 21, several cosmic runs with no  
217 magnetic field were taken to check the performance and compare them with corresponding ones  
218 for 2022 data samples. We observed no issues, in particular the noise distributions over readout  
219 channels remained basically unchanged as well as SNR for the clusters associated to the tracks, with  
220 stable excellent efficiency for all the sensors.

## 221 7. Conclusions

222 To conclude, SVD has successfully operated since March 2019 with very smooth performance  
223 and without major problems. Its good vertexing quality has been confirmed by many physics  
224 measurements, in particular those related to the lifetime analyses e.g. Ref. [9]. Some radiation  
225 damage effects were observed, but without any impact on the performance so far.



226 However, the extrapolated background level indicates that the occupancy in the SVD can exceed  
227 the current limit that **guarantees** good tracking performance. Hence, several software improvements  
228 are being implemented to account for high background conditions. In particular, exploitation of  
229 the SVD hit time is of major importance. Alongside, a VXD upgrade is also under discussion to  
230 increase robustness against high background and to match a possible new interaction region.

231 The VXD reinstallation at Belle II with complete PXD has been successfully done during the  
232 LS1, followed by successful VXD commissioning with cosmic data. The beam operation is planned  
233 to resume in early 2024.

## 234 **References**

- 235 [1] T. Abe et al., Belle II Technical Design Report, arXiv:1011.0352 (2010).  
236 [2] K. Adamczyk et al., JINST **17**, P11042 (2022).  
237 [3] M. J. French et al., Nucl. Instrum. Meth. A **466**, 359 (2001).  
238 [4] R. Turchetta, Nucl. Instrum. Meth. **335**, 1-2, pages 44-58 (1993).  
239 [5] G. Lindstrom et al., Nucl. Instrum. Meth. A **465**, 60-69 (2000).  
240 [6] B. Aubert et al., Nucl. Instrum. Meth. A **729**, 615 (2013).  
241 [7] A. Natochii et al., Nucl. Instrum. Meth. A **1055**, 168550 (2023).  
242 [8] M. Babeluk et. al., Nucl. Instrum. Meth. A **1048**, 168015 (2023).  
243 [9] F. Abudinén et al., Phys. Rev. Lett. **130**, 071802 (2023)